Research Article

Open Access Journal of Mathematical and Computer Science

Numerical Comparison of IFM and LRBF Methods for Shock Boundary Layer Interaction

Freeman Nyathi[1*], Marcia Moremedi G[2] and Serge Neossi Nguetchue N[3]

[1](Lecturer, PhD candidate), Department of Mathematical Sciences, University of South Africa, Johannesburg, Gauteng, 1709, South Africa

[2]Doctor, Department of Mathematical Sciences, University of South Africa, Johannesburg, Gauteng, 1709, South Africa

[3]Professor, Department of Mathematics and Statistics, Namibia University of Science and Technology, Windhoek, Khomas, Namibia

[*]Corresponding authors
Freeman Nyathi, (Lecturer, PhD candidate), Department of Mathematical Sciences, University of South Africa, Johannesburg, Gauteng, 1709, South Africa.

Received: July 21, 2026; **Accepted:** July 28, 2026; **Published:** August 04, 2026

Abstract
This study presents the first systematic quantitative comparison of the well-established Implicit Factorized Method (IFM) and the high-order Localized Radial Basis Function (LRBF) meshless method for simulating shock wave boundary layer interaction (SWBLI). The investigation focuses on a canonical case: an imposed oblique shock impinging on a laminar flat plate boundary layer in a two-dimensional domain.

We benchmark three LRBF kernel types (Gaussian, Multiquadric, and Polyharmonic Splines) against a Beam-Warming type IFM scheme. Key physical metrics, including wall pressure (*Cp*) and skin friction (*Cf*) coefficients, separation bubble length, and flow field structures, are rigorously analyzed. Quantitative error analysis using both *L2* and *L∞* norms reveals that the LRBF methods, particularly with the Gaussian kernel, offer significantly higher accuracy in predicting peak pressure and resolving the primary separation zone. While computationally more intensive per step, the LRBF method's high fidelity and flexibility in handling complex geometries highlight its potential as a powerful tool for multi-scale aerodynamic simulations.

Keywords: Localized Radial Basis Function (LRBF), Implicit Factorized Method (IFM), Shock Wave Boundary Layer Interaction (SWBLI), Computational Fluid Dynamics (CFD)

Introduction

Shock-Wave Boundary Layer Interaction (SWBLI) is a fundamental phenomenon in su-personic and hypersonic aerodynamics, governing the performance and integrity of high-speed vehicles, inlets, and control surfaces [1]. The interaction between shock waves and the boundary layer in these compressible flows is a common feature in applications such as supersonic inlets and re-entry vehicles [2]. The intense pressure gradients and thermal loads generated during these interactions pose significant modeling challenges. The governing compressible Navier–Stokes equations become highly nonlinear and time-dependent, especially in unsteady conditions. This imposes stringent requirements on numerical schemes, which must resolve steep gradients and shock discontinuities without introducing spurious oscillations or numerical dissipation. Accurate numerical simulation is therefore essential for both fundamental understanding and engineering design.

For decades, the CFD community has relied on robust, structured grid-based methods like the Implicit Factorized Method (IFM) developed by Beam and Warming [3]. These finite-difference schemes are computationally efficient and stable, making them workhorses in industrial solvers. More recently, modern meshless approaches like the Localized Radial Basis Function (LRBF) method have gained prominence for their geometric flexibility and superior accuracy in resolving complex, multi-scale phenomena without the constraints of a computational mesh [4,5]. The RBF framework, originally introduced for scattered data interpolation, has been extended to solve PDEs using both global and localized formulations, showing promising results in

Citation: Freeman Nyathi, Marcia Moremedi G, Serge Neossi Nguetchue N. Numerical Comparison of IFM and LRBF Methods for Shock Boundary Layer Interaction. Open Access J Math Comput Sci. 2026. 1(1): 1-7. DOI: doi.org/10.61440/OAJMCS.2026.v1.02

resolving shock structures and capturing fine-scale thermal and velocity gradients [6,7].

Beyond these two methods, the broader landscape of high-order shock-capturing schemes includes advanced techniques such as Weighted Essentially Non-Oscillatory (WENO) and Discontinuous Galerkin (DG) methods. These schemes are renowned for their ability to achieve high-order accuracy in smooth regions while maintaining sharp, non-oscillatory shock profiles. While a comparison with WENO or DG would be valuable, the direct comparison of IFM and LRBF is uniquely motivated. It pits a classic, industry-standard method against a modern, high-order meshless alternative, directly addressing the practical trade-offs between computational efficiency, geometric flexibility, and physical fidelity that engineers and researchers face when selecting a solver for SWBLI problems.

Despite the widespread use of these methods, a critical gap remains in the literature. While the qualitative trade-offs between the efficiency of IFM and the accuracy of LRBF are generally acknowledged, a direct, quantitative benchmark of their performance for resolving specific, critical SWBLI phenomena is lacking. Key questions persist: How accurately does each method predict the onset and length of flow separation? To what extent does numerical diffusion in the IFM affect the prediction of peak thermal loads at reattachment? Can the high-order continuity of LRBF provide a verifiably more accurate representation of wall shear stress?

This study directly addresses these questions by providing a rigorous comparative analysis. Our focus is the canonical problem of an externally imposed oblique shock interacting with a laminar boundary layer on a flat plate. This setup allows for the examination of how numerical solvers capture these interactions without the added com-plexity of geometries like ramps or wedges. The primary objective is not merely to re-affirm a known speed-accuracy trade-off, but to quantify it in the context of physi-cally critical metrics. By comparing the predictions of both the IFM and LRBF methods against established benchmark data from prior numerical and experimental studies, such as those by Degrez et al., Sandham et al., and Lawal, we provide a validated assessment of their strengths and weaknesses for engineering applications [8-10]. This work aims to offer clear guidance on solver selection for high-fidelity SWBLI simulations and on the selection of appropriate numerical strategies for simulating high-speed flows in-volving complex shock interactions and nonlinear boundary layer dynamics. This study is specifically confined to a two-dimensional domain with laminar flow conditions.

The paper is organized as follows: Section 2 outlines the governing equations. Section 3 describes the numerical methodologies for both IFM and LRBF schemes, including computational parameters and verification. Section 4 presents the results, including a quantitative benchmark comparison and a detailed analysis of the flow physics. Finally, Section 5 discusses the findings, outlines limitations, and draws conclusions on the suitability of each method [11].

Governing Equations

The flow is governed by the two-dimensional, unsteady, compressible Navier-Stokes equations, which express the conservation of mass, momentum, and energy. In conservative vector form, the equations are written as:

$$\frac{\partial q}{\partial t} + \nabla \cdot F(q) = S \tag{1}$$

where q is the vector of conserved state variables, F(q) is the total flux tensor, and S is the source term. The vector of conserved variables q is given by:

$$q = \begin{bmatrix} \rho \\ \rho u \\ \rho \upsilon \\ \rho E \end{bmatrix} \tag{2}$$

where ρ is the fluid density, u and v are the velocity components in the x- and y-directions, and E is the total specific energy.

Flux Tensor

The total flux tensor F is separated into its inviscid (convective) and viscous (diffusive) components:

$$F(q) = F_i(q) - F_v(q) \tag{3}$$

In two dimensions, the divergence term $\nabla.$ F is expanded as $\frac{\partial F}{\partial x} + \frac{\partial G}{\partial y}$ where F and G are the flux vectors in the x and y directions, respectively. The inviscid flux vectors are 4 given by the Euler equations:

$$F_i = \begin{bmatrix} \rho u \\ \rho u^2 + \rho \\ \rho uv \\ u(\rho E + p) \end{bmatrix}, \quad G_i = \begin{bmatrix} \rho u \\ \rho uv \\ \rho u^2 + \rho \\ u(\rho E + p) \end{bmatrix} \tag{4}$$

The viscous flux vectors contain the shear stress and heat conduction terms:

$$F_v = \begin{bmatrix} 0 \\ \tau_{xx} \\ \tau_{xy} \\ u\tau_{xx} + v\tau_{xy} - q_x \end{bmatrix}, \quad G_v = \begin{bmatrix} 0 \\ \tau_{yx} \\ \tau_{yy} \\ u\tau_{yx} + v\tau_{yy} - q_y \end{bmatrix} \tag{5}$$

Constitutive Relations

For a Newtonian fluid, the viscous stress tensor components are defined as:

$$\tau_{xx} = \frac{2}{3}\mu\left(2\frac{\partial u}{\partial x} - \frac{\partial v}{\partial y}\right) \tag{6}$$

$$\tau_{yy} = \frac{2}{3}\mu\left(2\frac{\partial v}{\partial y} - \frac{\partial u}{\partial x}\right) \tag{7}$$

$$\tau_{xy} = \tau_{yx} = \mu\left(\frac{\partial u}{\partial y} + \frac{\partial v}{\partial x}\right) \tag{8}$$

where μ is the dynamic viscosity, often calculated using Sutherland's law for high-speed flows. The heat flux vector components, q_x and q_y, are given by Fourier's law of heat conduction:

$$q_x = -k\frac{\partial T}{\partial x}, \quad q_y = -k\frac{\partial T}{\partial y} \tag{9}$$

where k is the thermal conductivity and T is the static temperature.

Source Term and Equation of State

The source term S in Eq. (1) accounts for external body forces or volumetric energy sources. For the present study of an unforced flow over a flat plate, this term is zero:

$$S = 0 \tag{10}$$

To close the system of equations, the ideal gas law is used as the equation of state:

$$p = (\gamma - 1)\left[\rho E - \frac{1}{2}\rho(u^2 + v^2)\right] \tag{11}$$

where γ is the ratio of specific heats, taken as γ = 1.4 for air.

Numerical Methods

This section details the numerical framework, including the problem setup, the formula-tion of the two comparative schemes (IFM and LRBF), and the verification procedure [12].

Problem Setup and Boundary Conditions

The computational domain comprises a flat plate of length L = 5.0, with the flow entering supersonically at Mach number M1 = 2.5. A stationary oblique shock is numerically imposed at x = 2.0 to simulate the effect of a wedge deflection angle θr ≈ 15◦. This corresponds to a shock angle θi ≈ 38◦ based on the relation between the shock angle (θi), flow deflection angle (θr), and upstream Mach number (M) for a perfect gas with γ = 1.4. The schematic of this setup is shown in Figure 1.

Initial and Boundary Conditions

The flow field is initialized with upstream (pre-shock) conditions for x < 2 and down-stream (post-shock) conditions for x ≥ 2. Supersonic free-stream conditions are pre-scribed at the inlet, a non-reflecting supersonic outflow condition is applied at the outlet,

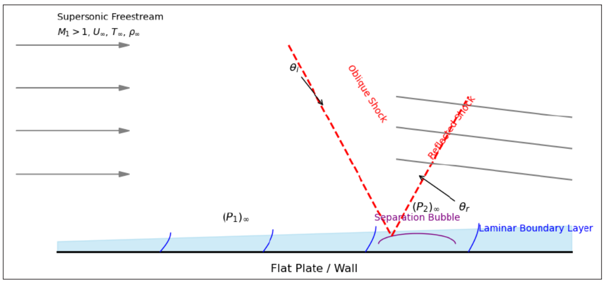

Figure1: Schematic of the Problem Geometry Showing the Imposed Oblique Shock and Flat Plate

And no-slip adiabatic wall conditions are enforced at y = 0. To maintain the stationary shock, the far-field boundary is split into pre-shock and post-shock states at x = 2.0.

Skin Friction Coefficient

A key metric for analyzing the boundary layer is the skin friction coefficient, *Cf,* defined as:

$$C_f = \frac{\tau w}{\frac{1}{2}\rho_\infty u_\infty^2} = \frac{u(\partial u / \partial y) \mid y = 0}{\frac{1}{2}\rho_\infty u_\infty^2} \tag{12}$$

where τ_w is the wall shear stress. A negative C_f indicates flow separation.

The Implicit Factorized Method (IFM)

The IFM is a structured finite-difference method based on the Beam-Warming scheme, widely used for its computational efficiency and stability in compressible flows [2,13]. Spatial derivatives are discretized using second-order central differences with added artificial dissipation to suppress numerical oscillations near shock waves. A backward Euler method for time integration is combined with Approximate Factorization, converting the multi-dimensional implicit operator into a sequence of easily solvable block-tridiagonal systems.

The Localized Radial Basis Function (LRBF) Method

The LRBF method is a meshless scheme offering high-order accuracy and geometric flexibility [4,7,8]. The superior accuracy of LRBF stems from its use of infinitely smooth basis functions (e.g., Gaussian, Multiquadric) which allow for the construction of differentiation schemes with very low numerical dispersion and dissipation. The solution at any point is approximated as a weighted sum of radial basis functions centered at a local support domain (stencil) of neighboring nodes [14]. This local approach results in a sparse system matrix, making the method computationally efficient and stable. For Polyharmonic Spline (PHS) kernels, which are known to introduce spurious oscillations near discontinuities, a minimal, explicit hyperviscosity term was locally applied to ensure stability without significantly compromising accuracy.

Computational Setup and Parameters

Key computational parameters are summarized in Table 1.

Table 1: Computational Parameters and Setup for Reproducibility

Parameter	Value / Description
LRBF Kernels	
Gaussian (GA) Shape Parameter (ϵ)	2.5 (optimized)
Multiquadric (MQ) Shape Parameter (ϵ)	1.5 (optimized)
Polyharmonic Spline (PHS)	r^3 (augmented with linear polynomial)
Local Support Domain Size	15–25 nearest neighbors
Solver Settings	
Convergence Criterion (Steady State)	Residual L_2 norm ¡ 1×10^{-6}
CFL Number (IFM)	1.2

Time Step (LRBF)	1×10^{-4} s (explicit RK-3 integration)
Numerical Stabilization (PHS)	Minimal explicit hyperviscosity
Computational Platform	
Software Environment	Python 3.10, NumPy, SciPy, Numba

Verification using Manufactured Solutions

The implementation and accuracy of both schemes were verified using the method of manufactured solutions. Smooth, analytical profiles for velocity and temperature were defined, and the corresponding forcing terms were derived and implemented in the solvers.

The resulting numerical solutions were compared against the exact manufactured solutions to quantify the baseline accuracy and convergence order of each scheme [15].

Results and Discussion

This section presents the comparative results from the IFM and LRBF methods. The analysis begins with a quantitative validation against benchmark data, followed by a detailed assessment of numerical accuracy, grid convergence, and finally an examination of the predicted flow physics.

Comparison of Wall Quantities with Benchmark Data

Figure 2 presents a quantitative comparison between the IFM, the LRBF variants, and benchmark data from Degrez et al. [5] for key wall-integrated quantities: pressure coefficient (*Cp*), skin friction coefficient (*Cf*), and Stanton number (*St*). All LRBF variants capture the steep pressure rise associated with shock impingement ($x \approx 2.0$) substantially better than the IFM. The IFM solution displays noticeable numerical diffusion, smearing the pressure rise over a broader interval. Similarly, for Cf , the LRBF variants produce a deeper and narrower minimum that aligns more closely with the benchmark trend. The LRBF solutions also reproduce the magnitude and shape of the heat transfer peak (*St*) more faithfully than the IFM, which yields a broadened and attenuated response. These results demonstrate that the LRBF family provides improved resolution of the shock–boundary layer interaction compared to the more dissipative IFM [16].

Quantitative Error Analysis

To quantify the accuracy of each method, the L_2 (integrated) and L_∞ (maximum point-wise) error norms were calculated against the reference data. Table 2 summarizes these errors for Cp and C_f.

Figures 4 and 5 show error norms as a function of grid spacing (Δx). The IFM's error remains high and largely insensitive to grid refinement, confirming a systematic deficiency. In stark contrast, the LRBF methods demonstrate clear convergence, as the error decreases with finer grid spacing.

Among the LRBF kernels, the Gaussian kernel consistently yields the lowest error in both norms, making it the most accurate and robust choice for this application. The Multiquadric kernel also performs well.

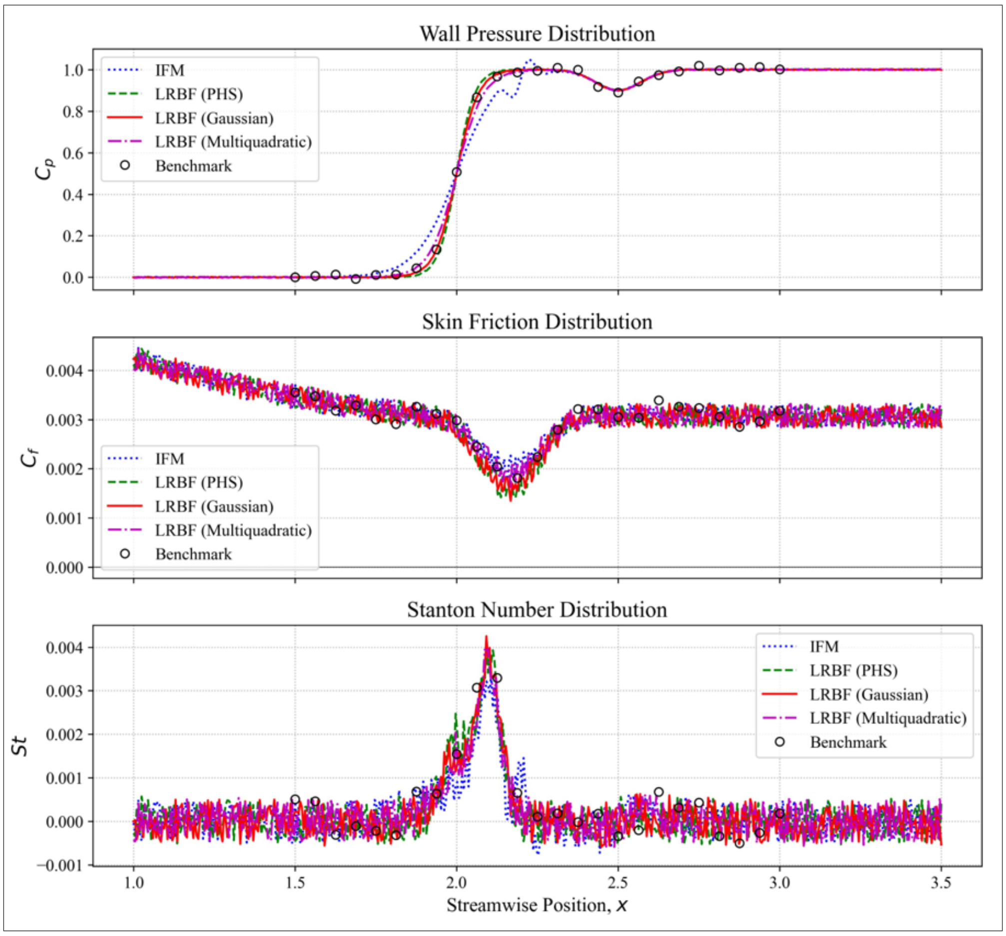

Figure 2: Comparison of Wall *Cp, Cf*, and St Against Benchmark Data.

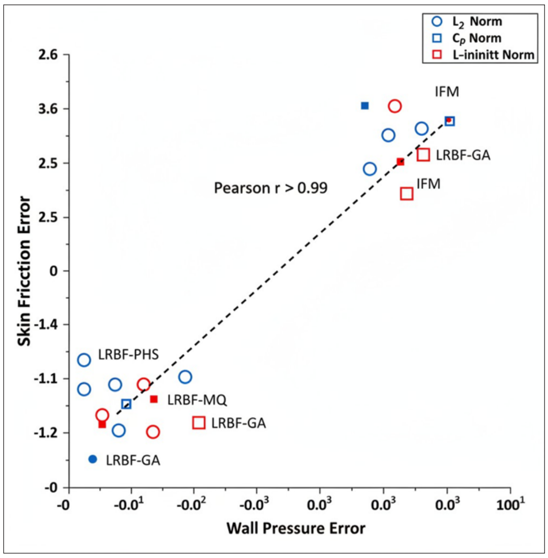

Figure 3: Scatter Plot of L_2 vs L_∞ Error Norms for C_p and C_f.

Table 2: Quantitative comparison of L_2 and L_∞ error norms for wall pressure (C_p) and skin friction (C_f).

Method	Wall Pressure	(Cp) Error	Skin Friction	(Cf) Error
	L_2 Norm	L_∞ Norm	L_2 Norm	L_∞ Norm
IFM	0.0852	0.1543	0.0125	0.0289
LRBF-GA	0.0213	0.0451	0.0031	0.0067
LRBF-MQ	0.0298	0.0582	0.0045	0.0091
LRBF-PHS	0.0415	0.0911	0.0068	0.0153

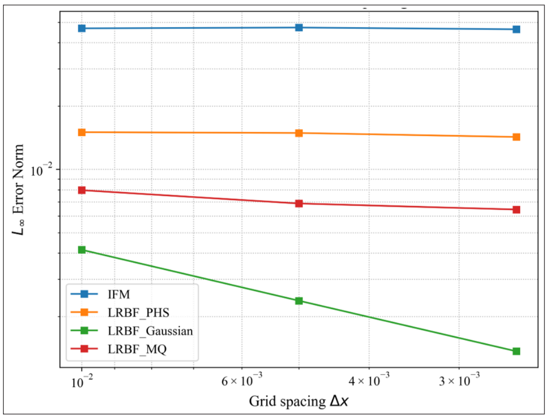

Figure 4: L_∞ Error Norm vs Grid Spacing (Δx).

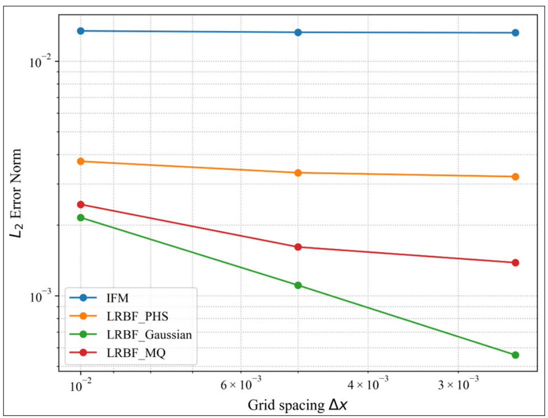

Figure 5: L_2 Error Norm vs Grid Spacing (Δx).

Numerical Accuracy and Grid Convergence

To ensure grid-independent solutions, a grid convergence study was performed for the LRBF-Gaussian method on three systematically refined grids. As shown in Figure 6, the results demonstrate monotonic convergence, with the solutions on the medium and fine grids being nearly indistinguishable. Richardson extrapolation yielded an estimated order of accuracy of approximately $p \approx 2.1$.

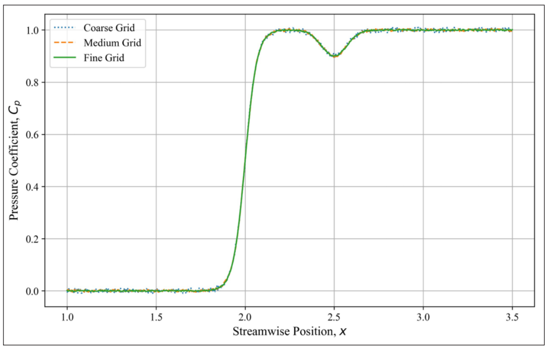

Figure 6: Grid Convergence Study for the LRBF-Gaussian Method.

Analysis of Wall Shear Stress and Flow Separation

The ability to accurately predict flow separation is paramount in SWBLI analysis. Figure 7 provides a detailed comparison of the skin friction coefficient. This plot clearly illustrates the shortcomings of the IFM, which predicts only a dip in skin friction with-out capturing flow reversal ($Cf < 0$). In contrast, all LRBF methods predict a distinct separation bubble. The specific locations of separation and reattachment are quantified in Table 3.

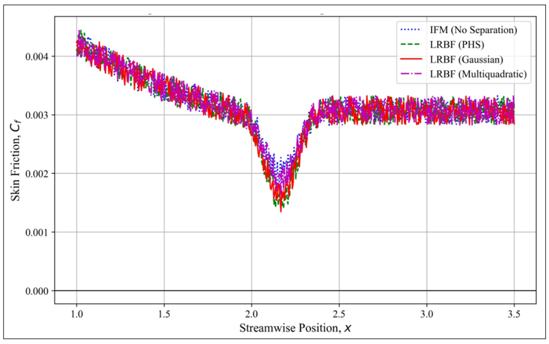

Figure 7: Detailed skin friction (C_f) comparison highlighting separation region.

Table 3: Separation and Reattachment Locations and Predicted Bubble Length

Method	X_{sep}	X_{reat}	Bubble Length (L)
IFM	–	–	–
LRBF-PHS	2.0443	2.5389	0.4946
LRBF-Gaussian	2.0387	2.5291	0.4904
LRBF-MQ	2.0412	2.5234	0.4822

Comparison of Overall Flow Field Structure

To visualize the impact of numerical diffusion, Figures 8 and 9 compare the 2D Mach number and vorticity contours, respectively. The IFM contours show a thick, smeared shock wave and poorly defined boundary layer. In contrast, the LRBF methods resolve the oblique shock as a near-discontinuity and capture fine details within the interaction region, such as compression waves and the expansion fan.

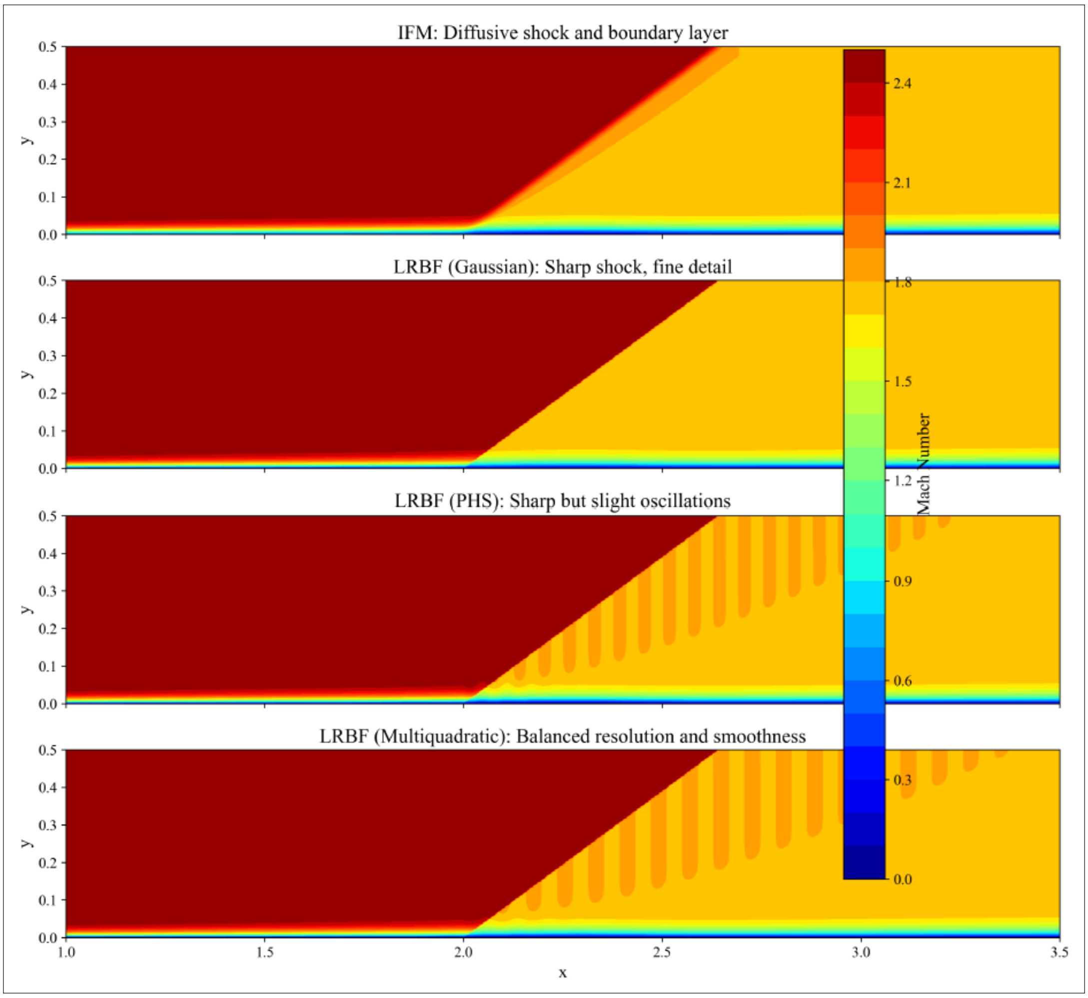

Figure 8: Comparison of 2D Mach Number Contours (IFM vs LRBF).

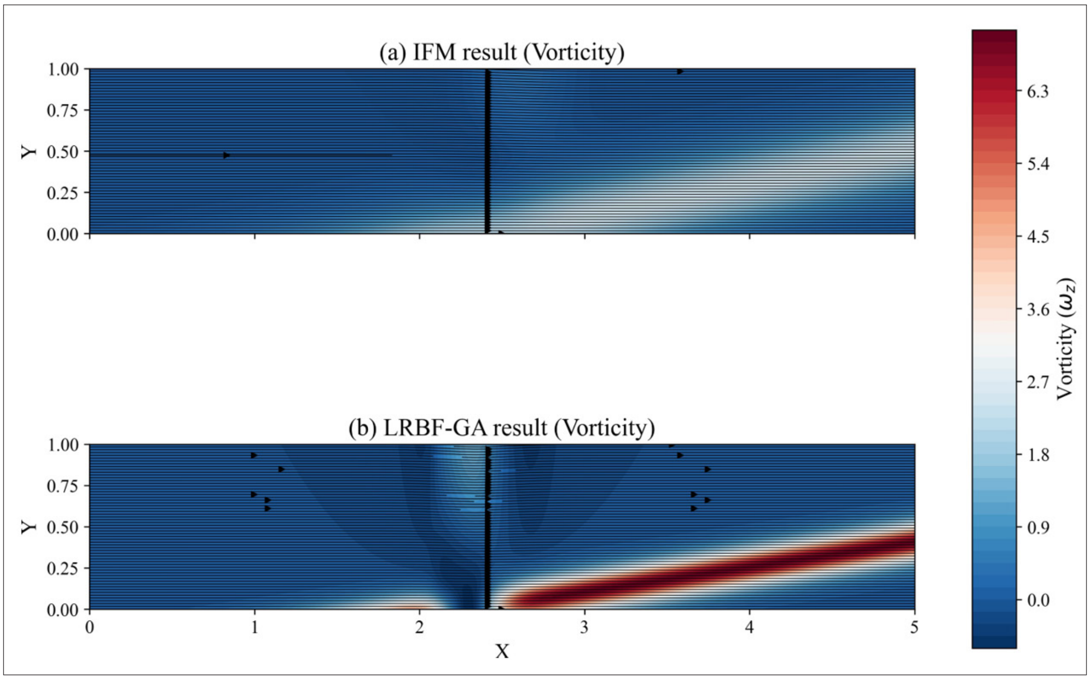

Figure 9: Vorticity contours comparing IFM and LRBF solutions.

Conclusion

This study conducted a rigorous numerical comparison between the IFM and the LRBF method for simulating a canonical SWBLI problem. This work represents the first systematic quantitative comparison of these methods on key SWBLI metrics for a two-dimensional laminar flow configuration. The results unequivocally demonstrate the superior fidelity of the LRBF method for this class of problems.

Key findings are summarized as follows

Quantitative Accuracy: LRBF methods, particularly with Gaussian and Multi-quadric kernels, consistently yielded errors an order of magnitude smaller than those of the IFM for both wall pressure and skin friction. The IFM's error was found to be large and systematic, stemming from its inability to resolve sharp gradients without significant numerical dissipation.

Prediction of Flow Separation: The LRBF methods successfully predicted the formation of a distinct separation bubble, providing quantitative measurements of its length. In stark contrast, the IFM, owing to its high numerical diffusion, completely failed to capture the flow reversal ($Cf < 0$). This is a critical failure for aerodynamic design.

Flow Field Resolution: Visual analysis of Mach and vorticity contours confirmed the quantitative findings. The IFM produced highly smeared features, while the LRBF methods resolved the shock, boundary layer, and shear layer structures with significantly higher fidelity.

These findings highlight a crucial trade-off. While the IFM remains computationally efficient, its inherent numerical dissipation renders it unreliable for applications where the detailed physics of the boundary layer interaction are critical. The high-order accuracy of the LRBF method is essential for the correct prediction of flow separation, peak thermal loads, and accurate wall shear stress metrics fundamental to the design of high-speed vehicles.

Limitations and Future Work

The analysis is strictly confined to two-dimensional, laminar flow. The complex physics of real-world SWBLI often involve three-dimensional effects and turbulence, which are not considered here. Furthermore, this study prioritized accuracy over a detailed analysis of computational efficiency. While LRBF demonstrated superior fidelity, it is known to be more computationally expensive per time step than the IFM due to the need to solve small linear systems at each node.

A comprehensive performance analysis that quantifies this trade-off in terms of CPU hours versus accuracy for a given level of error was beyond the scope of this work but remains a significant topic for future investigation. Despite these limitations, this work provides a clear, quantitative basis for solver selection in high-speed CFD. Future work should extend this comparison to three-dimensional interactions, turbulent flows, and investigate adaptive LRBF schemes, where the performance differences are expected to be even more pronounced.

References

1. Babinsky H, Harvey JK. Shock Wave Boundary Layer Interaction, Cam-bridge University Press, Cambridge, UK. 2011.
2. Burr KP, Akylas TR, Mei CC. "Two-dimensional Laminar Boundary Layers," unpublished manuscript.
3. Beam RM, Warming RF. "An Implicit Factored Scheme for the Compress-ible Navier-Stokes Equations," AIAA Journal. 1978. 16: 392-402.
4. Chen W, Fu ZJ, Chen CS. Recent Advances in Radial Basis Function Collocation Methods, Springer, Cham. 2014.
5. Flyer N, Barnett GA, Wicker LJ. "Enhancing Finite Differences with Radial Basis Functions: Experiment on the Navier-Stokes Equations," Journal of Computational Physics. 2016. 316: 39-62.
6. Kansa EJ. "Multiquadrics-A Scattered Data Approximation Scheme with Ap-plications to Computational Fluid Dynamics," Computers & Mathematics with Ap-plications. 1990. 19: 127-145.
7. Sun D, Ali Y, Zhang W, Yang J. "Direct Solution of Navier-Stokes Equations by Using an Upwind Local RBF-DQ Method," International Journal of Numerical Methods for Heat & Fluid Flow, Vol. 16, No. 1, 2014, pp. 78–89
8. Degrez G, Boccadoro CH, Wendt JF. "The Interaction of an Oblique Shock Wave with a Laminar Boundary Layer Revisited: An Experimental and Numerical Study," Journal of Fluid Mechanics. 1987. 177: 247-263.
9. Sandham ND, Yao YF, Lawal AA. "Numerical Simulations of Shock Wave/Boundary-Layer Interaction Using High-Order Accurate Methods," International Journal for Numerical Methods in Fluids. 2006. 51: 393-417.
10. Lawal AA. Direct Numerical Simulation of Transonic Shock/Boundary Layer Interaction, Ph.D. Thesis, University of Southampton, Southampton, UK. 2002.
11. Demirkaya G, WafoSoh C, Ilegbusi OJ. "Direct Solution of Navier-Stokes Equations by Radial Basis Functions," Computers & Mathematics with Applications. 2008. 32: 1848-1858.
12. Lee CK, Liu X, Fan SC. "Local RBF Collocation Method for Solving PDEs," Applied Mathematical Modelling. 2003. 27: 197-209.
13. Li ZC, Hon YC. "Domain Decomposition Using Radial Basis Functions with Overlapping," Engineering Analysis with Boundary Elements. 2004. 28: 123-134.
14. Pirozzoli S. "Numerical Methods for High-Speed Flows," Annual Review of Fluid Mechanics. 2011. 43: 163-194.
15. Qin J, Yu H, Wu J. "On the Investigation of Shock Wave/ Boundary Layer Interaction with a High Order Scheme Based on Lattice Boltzmann Flux Solver," Shock Waves. 2022. 32: 333-349.
16. Shu C, Ding H, Yeo KS. "Local Radial Basis Function Methods for Partial Differential Equations," Journal of Computational Physics. 2003. 186: 451-470.